Am J Transl Res 2026;18(8):6834-6849
www.ajtr.org /ISSN:1943-8141/AJTR0172347

Original Article

Yishen Quyu Lishi Formula suppresses multiple myeloma growth via ERK/mTOR-mediated inhibition of protective autophagy and induction of apoptosis

Juan Song[1], Hongyong Yang[2], Yifei Wang[3], Yuning Zhang[4], Xiujun Li[4]

[1]The First Clinical Medical School of Guangzhou University of Chinese Medicine, The Second Affiliated Hospital of Guizhou University of Traditional Chinese Medicine, Guangzhou 510405, Guangdong, China; [2]The First Affiliated Hospital of Guangzhou University of Chinese Medicine, Guangzhou 510405, Guangdong, China; [3]Guangzhou University of Chinese Medicine, Guangzhou 510006, Guangdong, China; [4]Hematology Department, Guihang Guiyang Hospital, Guiyang 550006, Guizhou, China

Received March 1, 2026; Accepted June 11, 2026; Epub August 15, 2026; Published August 30, 2026

Abstract: Objectives: To evaluate the anti-tumor effect of Yishen Quyu Lishi Formula (YSQYLSF) on multiple myeloma (MM) and to determine whether this effect is mediated by extracellular signal-regulated kinase/mammalian target of rapamycin (ERK/mTOR)-regulated protective autophagy and apoptosis. Methods: H929 xenograft-bearing nude mice were treated with YSQYLSF, bortezomib (BO), or their combination for 21 days. Tumor growth, body weight, histopathology, immunohistochemistry, reverse transcription quantitative polymerase chain reaction (RT-qPCR), Western blotting, and ribonucleic acid sequencing (RNA-Seq) were performed. H929 cells were further used for cell viability assays, green fluorescent protein-microtubule-associated protein 1 light chain 3 (GFP-LC3) imaging, flow cytometry, Western blotting, and rapamycin rescue assays. Results: YSQYLSF reduced xenograft growth and, when combined with BO, produced a potent anti-tumor effect without significant weight loss or obvious liver and kidney damage. RNA-Seq identified 802 differentially expressed genes, with enrichment in mitogen-activated protein kinase (MAPK), mammalian target of rapamycin (mTOR), autophagy, apoptosis, inflammatory, and immune-related pathways. YSQYLSF increased the phosphorylated ERK/ERK and phosphorylated mTOR/mTOR ratios, decreased LC3-II/LC3-I, increased p62 accumulation, and enhanced the Bax/Bcl-2 and cleaved caspase-3/caspase-3 ratios. In vitro, YSQYLSF reduced H929 cell viability, decreased autophagosome formation, and promoted apoptosis. Rapamycin partially restored autophagy and attenuated apoptosis. Conclusions: YSQYLSF inhibits MM growth by activating the ERK/mTOR pathway, suppressing protective autophagy, and promoting mitochondrial apoptosis. Transcriptomic data also suggest additional immune- and inflammation-related mechanisms that require further validation.

Keywords: Yishen Quyu Lishi Formula, multiple myeloma, extracellular signal-regulated kinase/mammalian target of rapamycin signaling, protective autophagy, apoptosis, transcriptomic analysis

Introduction

Multiple myeloma (MM) is a hematologic malignancy characterized by the clonal proliferation of plasma cells and occurs mainly in older adults [1]. Although new therapeutic agents, including proteasome inhibitors, immunomodulatory drugs, and monoclonal antibodies, have improved patient survival, relapse and drug resistance remain major causes of treatment failure in MM [2, 3]. Therefore, identifying key molecular events involved in MM progression and developing new therapeutic strategies remain important clinical priorities.

Autophagy and apoptosis are closely linked to the survival advantage of MM cells. Because MM cells continuously synthesize large amounts of immunoglobulins and are exposed to persistent stress in the bone marrow microenvironment, they are highly dependent on basal autophagy. Protective autophagy helps MM cells tolerate metabolic and proteotoxic stress; when this process is disrupted, MM cells become more susceptible to pro-apoptotic signals [4]. The extracellular signal-regulated kinase/mammalian target of rapamycin (ERK/mTOR) pathway participates in cell proliferation, metabolic adaptation, autophagy, and cell death. In tumor

https://doi.org/10.62347/EGUV4191

biology, ERK/MAPK signaling is often regarded as a pro-survival and pro-proliferative pathway, but its biological function is context dependent. Under intense or sustained stress, ERK signaling can be involved in mitochondrial cell death and the regulation of cytoprotective autophagy. Therefore, the significance of ERK/mTOR activation in MM should be interpreted together with changes in autophagy and apoptosis rather than simply as an oncogenic event.

In traditional Chinese medicine, MM is commonly classified under the categories of Bone Bi, Bone Wei, and Xu Lao. Its pathogenesis is considered to involve kidney deficiency as the root cause, blood stasis as the major pathological basis, and toxin accumulation as an important contributing factor. Yishen Quyu Lishi Formula (YSQYLSF) was developed based on this pathophysiological understanding. Clinically, YSQYLSF has been used to relieve pain, abdominal distension, fatigue, edema, and other MM-related symptoms and may reduce chemotherapy-associated adverse effects [5, 6]. As a compound traditional Chinese medicine formula, YSQYLSF contains multiple medicinal materials and may exert synergistic effects through multi-component and multi-target regulation while reducing toxicity. However, the molecular basis of these effects remains unclear. Previous network pharmacology analysis suggested that YSQYLSF may exert anti-MM activity by regulating autophagy- and apoptosis-related pathways, but this hypothesis requires biological validation. RNA-Seq can comprehensively profile drug-induced transcriptional changes and is therefore suitable for investigating the molecular targets and mechanisms of compound formulas.

In this study, we combined in vivo efficacy and safety evaluation, transcriptomic profiling, and cell-based mechanistic experiments to clarify the anti-MM effects of YSQYLSF and the underlying mechanisms. First, we evaluated the antitumor activity and safety of YSQYLSF in a xenograft model. Second, RNA-Seq was performed to systematically analyze drug-induced changes in gene expression profiles and identify key signaling pathways. Third, cellular experiments were conducted to validate the effects of YSQYLSF on proliferation, autophagy, and apoptosis. These findings provide experimental evidence supporting the potential clinical application of YSQYLSF in MM treatment.

Materials and methods

Animals and cell lines

Thirty specific pathogen-free (SPF) female BALB/c nude mice aged 4-5 weeks and weighing 18-22 g were obtained from the Laboratory Animal Center of Shenzhen Lingfu Top Biotechnology Co., Ltd. [Animal Production License No.: SYXK (Guangdong) 2022-0293 (Guangming)]. All nude mice were housed in individually ventilated cages under SPF barrier conditions at 22 ± 2°C and 50 ± 10% relative humidity with a 12-h light/dark cycle. The animal protocol was reviewed and approved by the Institutional Animal Care and Use Committee of Guizhou University of Traditional Chinese Medicine (Approval No.: 20250409003).

The human MM cell line H929 was purchased from Shenzhen Lingfu Top Biotechnology Co., Ltd. Cells were maintained in Roswell Park Memorial Institute 1640 (RPMI-1640) complete medium supplemented with 10% fetal bovine serum (FBS) and 1% penicillin-streptomycin.

Preparation of experimental drugs

YSQYLSF: The formula consisted of Sangjisheng (Taxillus chinensis) 30 g, Buguzhi (Psoralea corylifolia) 10 g, Jixueteng (Spatholobus suberectus) 30 g, Banzhilian (Scutellaria barbata) 30 g, Tubiechong (Eupolyphaga sinensis) 10 g, and Bixie (Dioscorea hypoglauca) 15 g. All herbs were obtained from the Pharmacy of the First Affiliated Hospital of Guangzhou University of Chinese Medicine and were verified to meet the requirements of the Chinese Pharmacopoeia. The herbs were weighed according to the formula ratio, soaked in eight volumes of deionized water for 30 min, decocted for 1 h, filtered, and then decocted twice more. The combined filtrate was concentrated by rotary evaporation to 2.0 g/mL for in vivo use and 1.0 g/mL for in vitro use, aliquoted, and stored at -20°C.

Bortezomib (BO): Bortezomib lyophilized powder was dissolved in sterile injectable normal saline to prepare a stock solution, aliquoted, and stored at -20°C. Before use, aliquots were thawed and diluted with sterile normal saline to a working dose of 0.5 mg/kg body weight. The working solution was prepared under sterile conditions, protected from light, and used immediately.

3-MA (1.25 M): 50 mg of 3-MA powder was dissolved in 268.20 μL DMSO, aliquoted and stored at -20°C.

Bafilomycin A1 (Baf-A1, 0.5 mM): 31.14 μg of Baf-A1 was dissolved in 100 μL DMSO, aliquoted and stored at -20°C.

Rapamycin (10 mM): 5 mg of rapamycin was dissolved in 546.94 μL DMSO, aliquoted and stored at -20°C.

Experimental grouping and administration protocol

After the xenograft model was established, 20 tumor-bearing nude mice were randomly assigned to four groups (n = 5 per group) using a randomized block design: Model group, YSQYLSF group, BO group, and YSQYLSF+BO group. An additional blank control group (Control, n = 5) was established. Administration began on the day after grouping (day 0) and continued for 21 consecutive days: (1) Control and Model groups: 0.2 mL of sterile deionized water was administered by gavage once daily. (2) YSQYLSF group: 0.2 mL of YSQYLSF solution (1.5 g crude drug/mL) was administered by gavage once daily, equivalent to 0.3 g crude drug per mouse. (3) BO group: Bortezomib (0.5 mg/kg) was administered subcutaneously twice weekly (Monday and Thursday). (4) YSQYLSF+BO group: YSQYLSF was administered by daily gavage, and bortezomib was injected twice weekly at the same doses used in the monotherapy groups.

The general condition of the mice was monitored daily, and body weight and tumor size were measured every three days and recorded for growth-curve analysis.

Establishment of the H929 xenograft tumor model

Logarithmic-phase H929 cells were collected, washed, and resuspended in PBS at a final concentration of 5×10^7 cells/mL. For tumor transplantation, 0.2 mL of the cell suspension, containing approximately 1×10^7 cells, was injected subcutaneously into the left axillary region of each nude mouse. Mice in the blank control group were injected with the same volume of PBS. Tumor growth was first observed on day 6 after inoculation. Every three days, the longest and shortest tumor diameters were measured with calipers and recorded as a and b, respectively. Tumor volume was calculated using the following formula: $V = a \times b^2/2$.

Sample collection and processing: At the end of the 21-day treatment period, mice were euthanized by intraperitoneal injection of an overdose of pentobarbital sodium (150 mg/kg), followed by cervical dislocation as a secondary method to confirm death. Death was confirmed by the absence of spontaneous breathing, heartbeat, corneal reflex, and pedal withdrawal reflex for at least 5 min. Tumor tissues were collected and weighed accurately. Tumor growth inhibition (TGI) was calculated as follows: TGI (%) = [1 - mean tumor weight in the treatment group/mean tumor weight in the Model group] × 100%. Each tumor sample was divided into two portions. One portion was fixed in 4% paraformaldehyde for histopathology and immunohistochemistry, and the other portion was immediately frozen in liquid nitrogen and stored at -80°C for subsequent molecular analysis.

Transcriptomic sequencing (RNA-Seq) and bioinformatics analysis: Total ribonucleic acid (RNA) was extracted from tumor tissues from the Model and YSQYLSF groups. After quality control, libraries were prepared, and paired-end sequencing was performed on the Illumina NovaSeq 6000 platform. Clean reads were aligned to the human reference genome GRCh38 to capture transcriptional changes in H929 tumor cells. Because xenograft tumor tissues may contain host stromal or innate immune cells, the potential contribution of tumor-infiltrating microenvironmental cells to immune and inflammatory pathway enrichment was considered in the Discussion. DESeq2 was used for differential expression analysis with thresholds of $|\log_2(\text{fold change})| > 1$ and adjusted P value < 0.05. Differentially expressed genes (DEGs) were subjected to Gene Ontology (GO), Kyoto Encyclopedia of Genes and Genomes (KEGG), and gene set enrichment analysis (GSEA) using clusterProfiler.

Histological examination: H&E staining and immunohistochemistry (IHC): Tumor, liver, and kidney tissues were collected after the final treatment, fixed in 4% paraformaldehyde for 24 h, dehydrated, embedded in paraffin, and

cut into 4-μm-thick sections. Hematoxylin and eosin (H&E) staining was performed to evaluate tissue morphology. Immunohistochemistry (IHC) was used to detect cluster of differentiation 138 (CD138), LC3B, and cleaved caspase-3 expression. Images were acquired under identical settings. The positive staining area and mean optical density were quantified using Image-Pro Plus 6.0. H&E sections were semi-quantitatively scored by two blinded investigators for tumor necrosis, liver injury, and renal tubular injury, and the quantification was added to the revised **Figure 2**.

RT-qPCR analysis: TRIzol reagent was used to extract total RNA from tumor tissues. RNA quality was assessed, and complementary DNA (cDNA) was synthesized. Real-time RT-qPCR was performed using TB Green Premix Ex Taq II, with beta-actin used as the internal reference gene. The relative messenger RNA (mRNA) expression levels of mTOR, LC3, ERK, and p62 were calculated using the 2^-ΔΔCt method.

Western blot analysis: Total protein was extracted from tumor tissues and cells using radioimmunoprecipitation assay lysis buffer, and protein concentration was determined using a bicinchoninic acid assay. Equal amounts of protein were separated by sodium dodecyl sulfate-polyacrylamide gel electrophoresis and transferred to polyvinylidene fluoride membranes. After blocking, membranes were incubated overnight at 4°C with primary antibodies against p62, LC3B, Bax, Bcl-2, caspase-3, cleaved caspase-3, mTOR, phosphorylated mTOR, ERK1/2, phosphorylated ERK1/2, and beta-actin. Horseradish peroxidase-conjugated secondary antibodies were then applied for 1 h at room temperature, followed by enhanced chemiluminescence detection. Band intensity was analyzed using Image Lab software.

In vitro cellular assays

MTT assay for cell viability: H929 cells were seeded in 96-well plates (1×10^4 cells/well) and treated with YSQYLSF at crude drug-equivalent concentrations of 0, 1, 2, 4, 8, and 16 mg/mL for 36 or 48 h. MTT solution (15 μL, 5 mg/mL) was added to each well and incubated at 37°C for 4 h. After centrifugation and supernatant removal, 150 μL of dimethyl sulfoxide (DMSO) was added to dissolve the formazan crystals. Absorbance was measured at 490 nm. The in vitro IC50 value was expressed as the crude drug-equivalent concentration and was not interpreted as an achievable plasma concentration in vivo.

GFP-LC3 transfection for autophagosome detection: H929 cells were seeded in 6-well plates and infected for 24 h with adenovirus expressing green fluorescent protein-microtubule-associated protein 1 light chain 3 (Ad-GFP-LC3; multiplicity of infection = 10-50). After treatment with different concentrations of YSQYLSF for 36 h, cells were collected and prepared for confocal microscopy. GFP-LC3 puncta were counted using ImageJ software in at least five random fields per group.

Flow cytometry for apoptosis detection: H929 cells were treated with YSQYLSF for 36 h and stained using an Annexin V-fluorescein isothiocyanate/propidium iodide (Annexin V-FITC/PI) double-staining kit. Early apoptosis, late apoptosis, and total apoptosis rates were quantified by flow cytometry, and the quantified bar graph was added to the revised **Figure 6A**.

Western blot analysis of protein expression: Total protein was extracted from tumor tissues or cells, quantified by BCA assay, separated by sodium dodecyl sulfate-polyacrylamide gel electrophoresis, and transferred to PVDF membranes. Membranes were blocked with 5% nonfat dry milk, incubated with primary antibodies overnight at 4°C, incubated with secondary antibodies at room temperature for 1 h, and then developed using ECL chemiluminescence. Band intensity was analyzed using Image Lab software.

Statistical analysis

All data were analyzed using SPSS 27.0, and results are presented as mean ± standard deviation. Normality and homogeneity of variance were assessed before parametric testing. One-way analysis of variance followed by Tukey's multiple-comparison test was used for multiple-group comparisons, whereas Welch's analysis of variance or Games-Howell post-hoc tests were applied when variances were unequal. Repeated-measures data were analyzed using repeated-measures ANOVA. $P < 0.05$ was considered statistically significant. Figures were generated using GraphPad Prism 9.0.

Results

In vivo experimental results

General condition of tumor-bearing mice and model validation: On day 14 after inoculation, palpable masses were detected at the injection site in the left forelimb of all experimental nude mice, with minimum short-axis diameters > 10 mm. Some tumor surfaces showed ulceration and scabbing. CD138 immunohistochemical staining showed that the subcutaneous masses were CD138-positive plasma cell-derived tumors, confirming the successful establishment of the H929 MM xenograft model (**Figure 1A**).

YSQYLSF inhibits xenograft tumor growth: Tumor volumes were comparable among the Model, YSQYLSF, BO, and YSQYLSF+BO groups at baseline ($P > 0.05$). All treatment groups showed significantly slower tumor growth than the Model group during treatment. YSQYLSF reduced tumor size, BO showed a stronger inhibitory effect, and the combination group exhibited the greatest suppression of xenograft growth. At the end of the study, tumor weight reduction was 49.88% in the YSQYLSF group, 60.86% in the BO group, and 85.68% in the combination group (**Figure 1B-E**).

Effects of YSQYLSF on body weight in tumor-bearing mice: Body weight did not differ significantly among groups before modeling ($P > 0.05$). After 21 days of treatment, mice in the YSQYLSF, BO, and YSQYLSF+BO groups maintained better body-weight gain than mice in the Model group, with the most pronounced increase observed in the combination group (**Figure 2A**). These results indicate that YSQYLSF and BO were well tolerated in this study.

Effects of YSQYLSF on tumor and organ tissue morphology: H&E staining showed densely arranged tumor cells and necrotic areas in the Model group. YSQYLSF and BO reduced tumor cell density and necrosis, whereas the combination group showed the most obvious histological improvement. Quantitative analysis of the tumor necrotic area was added to **Figure 2B**.

In liver tissues, the Model group showed focal hepatocellular injury and inflammatory infiltration, whereas the YSQYLSF, BO, and combination groups exhibited milder pathological changes. Kidney tissues showed mild renal tubular dilation in the Model group, whereas the treatment groups had relatively intact glomeruli and tubules. Semi-quantitative liver and kidney injury scores were added to **Figure 2C**, **2D**, supporting the absence of obvious hepatorenal toxicity.

Transcriptomic sequencing analysis results

Screening of differentially expressed genes: Transcriptomic sequencing generated high-quality clean reads with mapping rates > 90%. Using $|\log_2(\text{fold change})| \geq 1$ and adjusted $P < 0.05$ as the criteria, 802 differentially expressed genes (DEGs) were identified, including 524 downregulated genes and 278 upregulated genes. A volcano plot was used to show the distribution of gene expression differences between the two groups; red dots represented significantly upregulated genes, and green dots represented significantly downregulated genes. Cluster heatmap analysis showed that samples from the Model and YSQYLSF groups formed distinct clusters based on gene expression profiles, with good intra-group reproducibility and significant inter-group differences (**Figure 3A**, **3B**).

GO functional enrichment analysis: GO functional enrichment analysis showed that, at the biological process (BP) level, DEGs were mainly enriched in the regulation of apoptotic process (GO:0016265), autophagy (GO:0006914), regulation of cell proliferation, inflammatory response (GO:0006954), and immune response. Apoptosis-related terms contained many upregulated genes, whereas autophagy-related terms had a higher proportion of downregulated genes. At the cellular component (CC) level, genes were significantly enriched in mitochondria (GO:0005739), endoplasmic reticulum, lysosome (GO:0005764), and plasma membrane. At the molecular function (MF) level, genes were enriched in protein kinase activity (GO:0004672), protein binding (GO:0005515), transcription factor activity, and enzyme regulator activity (**Figure 3C**).

KEGG signaling pathway and GSEA enrichment analysis: KEGG pathway enrichment analysis showed that the DEGs were mainly involved in three categories: environmental information

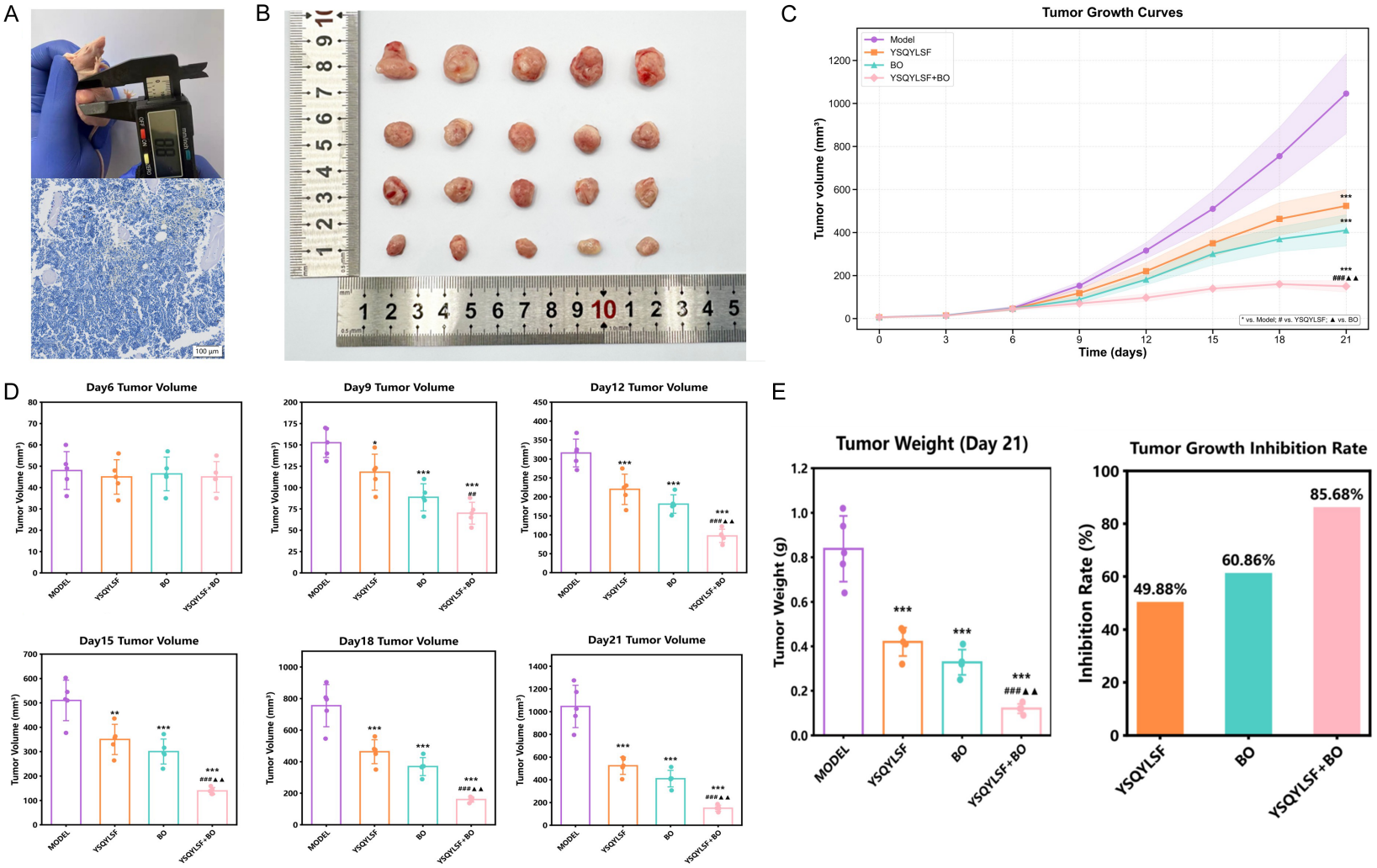

Figure 1. Effects of Yishen Quyu Lishi Formula (YSQYLSF) and bortezomib (BO) on H929 xenograft tumor growth in nude mice. A. Establishment and validation of the H929 xenograft model. B. Representative images of excised tumors at the study endpoint. C. Tumor growth curves. D. Tumor volume quantification. E. Tumor growth inhibition rate. Data are presented as the mean ± SD (n = 5). *P < 0.05, **P < 0.01, and ***P < 0.001 vs. the Model group; ##P < 0.01, and ###P < 0.001 vs. the YSQYLSF group; ΔP < 0.05, ΔΔP < 0.01 vs. the BO group.

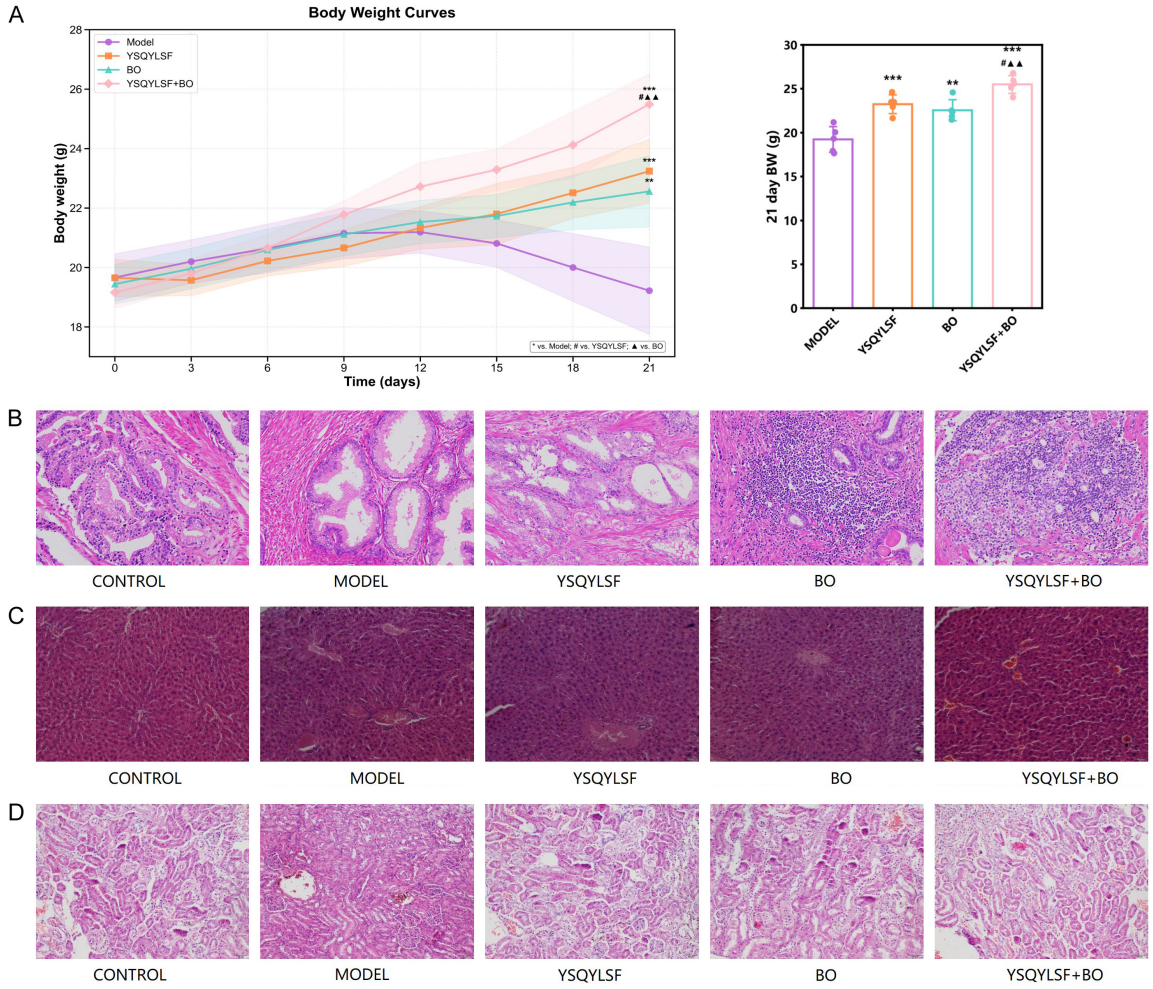

Figure 2. Effects of YSQYLSF and BO on body weight and histomorphology in H929 xenograft-bearing nude mice. A. Body-weight curves. B. Representative tumor hematoxylin and eosin (H&E) staining and quantitative tumor necrosis analysis. C. Representative liver H&E staining and semi-quantitative liver injury score. D. Representative kidney H&E staining and semi-quantitative renal tubular injury score. Scale bar = 100 μm; original magnification, ×200. Quantification was performed on at least five random fields per sample by two blinded investigators. Data are presented as the mean ± SD (n = 5). **P < 0.01, and ***P < 0.001 vs. the Model group; #P < 0.05 vs. the YSQYLSF group; ΔΔP < 0.01 vs. the BO group.

processing pathways, including MAPK, mTOR, and tumor necrosis factor signaling; cellular process pathways, including apoptosis, autophagy, and cell-cycle regulation; and organismal system pathways, including interleukin-17 and Toll-like receptor signaling (**Figure 3D**). These immune- and inflammation-related pathways were not treated as incidental findings but were further discussed as possible tumor cell-intrinsic inflammatory programs or microenvironment-associated responses in xenograft tissues.

GSEA showed that the apoptosis pathway (mmu04210) exhibited significant negative enrichment (NES = -2.74, P < 0.001), the mTOR signaling pathway (mmu04150) showed significant positive enrichment (NES = 2.00, P < 0.001), and the autophagy-related pathway (mmu04140) showed significant negative enrichment (NES = -1.86, P < 0.001) (**Figure 3E**).

Effects on autophagy-related gene and protein expression: RT-qPCR results showed that, compared with the Model group, mTOR and ERK mRNA expression levels in tumor tissues from the YSQYLSF, BO, and combination groups were significantly increased (P < 0.01 or P < 0.001), LC3 mRNA expression was significantly decreased (P < 0.01 or P < 0.001), and p62 mRNA

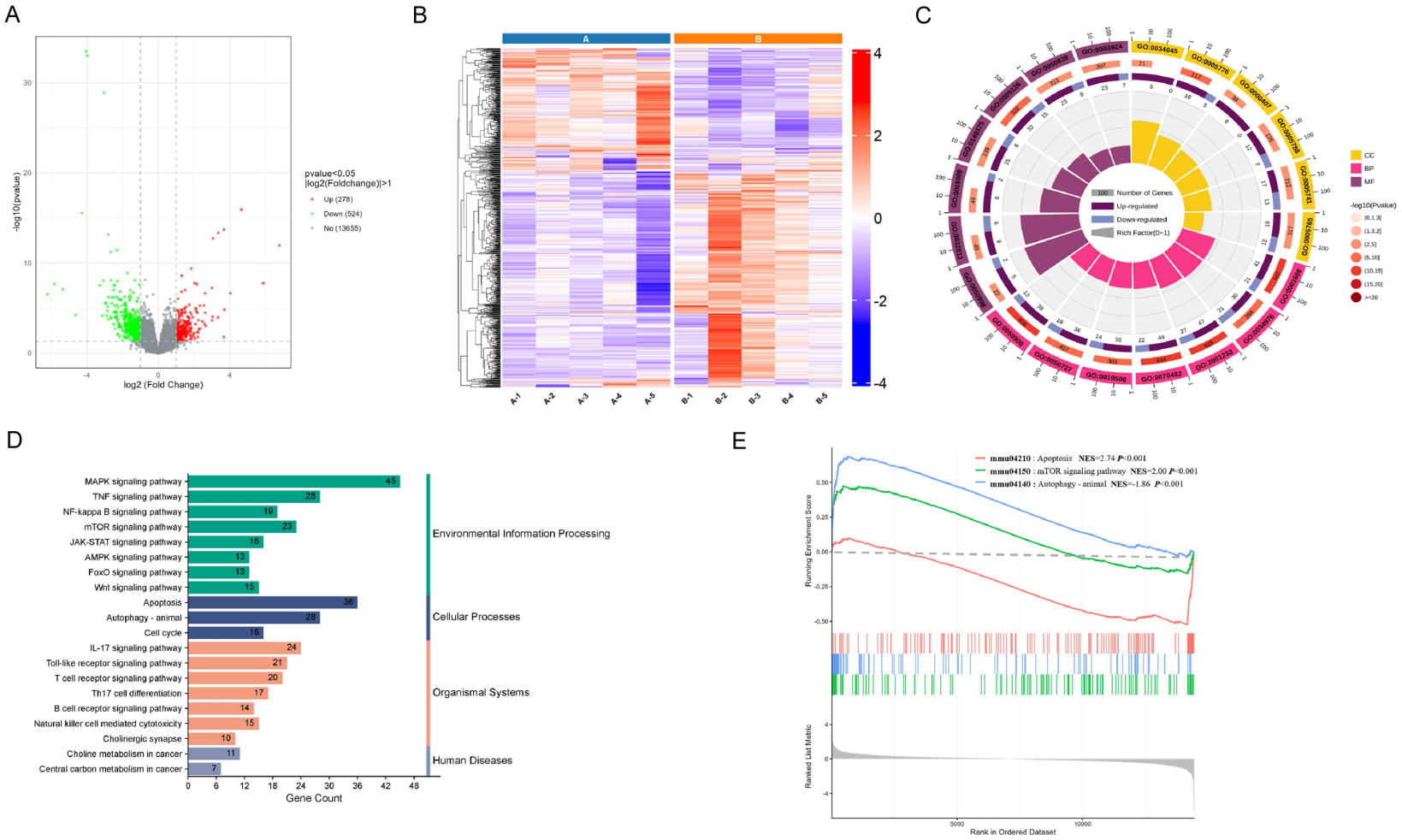

Figure 3. Transcriptomic analysis of tumor tissues from the YSQYLSF and Model groups. A. Volcano plot of differentially expressed genes (DEGs). B. Cluster heatmap of DEGs. C. Gene Ontology (GO) enrichment analysis. D. Kyoto Encyclopedia of Genes and Genomes (KEGG) pathway enrichment analysis. E. Gene set enrichment analysis (GSEA) of key pathways.

expression was significantly increased ($P < 0.01$ or $P < 0.001$). The combination group regulated these genes more significantly than the monotherapy groups ($P < 0.05$, $P < 0.01$, or $P < 0.001$) (**Figure 4C**).

Western blot analysis showed that the expression level of the autophagy substrate protein p62 was significantly increased in all treatment groups ($P < 0.01$ or $P < 0.001$), whereas the LC3-II/LC3-I ratio, a key autophagy index, was significantly decreased ($P < 0.001$) (**Figure 4D**). Immunohistochemistry showed strong positive LC3 expression in tumor tissues from the Model group, whereas LC3 expression was markedly weakened in all treatment groups, with the weakest expression observed in the combination group (**Figure 4A**). Semi-quantitative analysis showed that LC3 protein expression was significantly lower in all treatment groups than in the Model group ($P < 0.05$).

Effects on apoptosis-related protein expression: Western blot analysis revealed that, compared with the Model group, the ratio of the pro-apoptotic protein Bax to the anti-apoptotic protein Bcl-2 was significantly increased in all treatment groups ($P < 0.001$), and the ratio of cleaved caspase-3 to caspase-3 was also significantly increased ($P < 0.01$ or $P < 0.001$). The combination group was more effective than the monotherapy groups in promoting apoptosis ($P < 0.05$ or $P < 0.01$) (**Figure 4E**).

Immunohistochemistry showed weak positive cleaved caspase-3 expression in tumor tissues from the Model group, whereas cleaved caspase-3 expression was significantly enhanced in all treatment groups. The combination group showed the strongest expression, with widely distributed positive cells (**Figure 4B**).

Effects on ERK/mTOR signaling pathway-related protein expression: Western blot analysis demonstrated that, compared with the Model group, the p-mTOR/mTOR and p-ERK/ERK ratios in tumor tissues from the YSQYLSF, BO, and combination groups were significantly increased ($P < 0.01$ or $P < 0.001$) (**Figure 4F**), suggesting that YSQYLSF may activate ERK/mTOR signaling.

In vitro experimental results

Effects of YSQYLSF on H929 cell proliferation: MTT assay showed that YSQYLSF inhibited H929 cell viability in a concentration- and time-dependent manner. The 36-h and 48-h IC50 values were 6.36 and 3.91 mg/mL, respectively (**Figure 5A**). These values represent crude drug-equivalent concentrations used for in vitro screening and should not be directly interpreted as plasma concentrations after oral administration in vivo.

Effects of YSQYLSF on H929 cell autophagy: Ad-GFP-LC3 adenovirus transfection experiments showed that control H929 cells contained an average of 57.22 ± 5.07 autophagosomes per cell. After YSQYLSF intervention, the number of autophagosomes decreased significantly in a dose-dependent manner: 43.35 ± 4.54 autophagosomes/cell in the 1 mg/mL group, 32.57 ± 3.28 autophagosomes/cell in the 2 mg/mL group, and 19.95 ± 3.55 autophagosomes/cell in the 4 mg/mL group. All YSQYLSF-treated groups differed significantly from the control group ($F = 43.27$, $P < 0.001$) (**Figure 5B**).

As shown by Western blot analysis, with increasing YSQYLSF concentrations, p62 protein expression was significantly upregulated ($F = 63.55$, $P < 0.001$), whereas the LC3-II/LC3-I ratio was significantly decreased ($F = 41.29$, $P < 0.001$) (**Figure 5C**). Similar to the early-stage autophagy inhibitor 3-MA, YSQYLSF significantly decreased the LC3-II/LC3-I ratio, whereas the late-stage autophagy inhibitor Baf-A1 significantly increased this ratio. The YSQYLSF+Baf-A1 combination group showed no significant difference in the LC3-II/LC3-I ratio compared with the Baf-A1 group (**Figure 5D**), suggesting that YSQYLSF inhibits the upstream stage of autophagosome formation rather than autophagosome-lysosome fusion.

Effects of YSQYLSF on H929 cell apoptosis: Flow cytometry showed that the spontaneous apoptosis rate in control H929 cells was 4.43 ± 0.79%. After YSQYLSF treatment, the total apoptosis rate increased in a dose-dependent manner: 22.86 ± 3.06% in the 1 mg/mL group, 32.69 ± 4.08% in the 2 mg/mL group, and 48.25 ± 5.55% in the 4 mg/mL group ($F = 70.41$, $P < 0.001$) (**Figure 6A**). Western blot analysis demonstrated that YSQYLSF significantly altered the Bcl-2 family protein profile by upregulating the pro-apoptotic protein Bax and downregulating the anti-apoptotic protein Bcl-2, thereby significantly increasing the Bax/

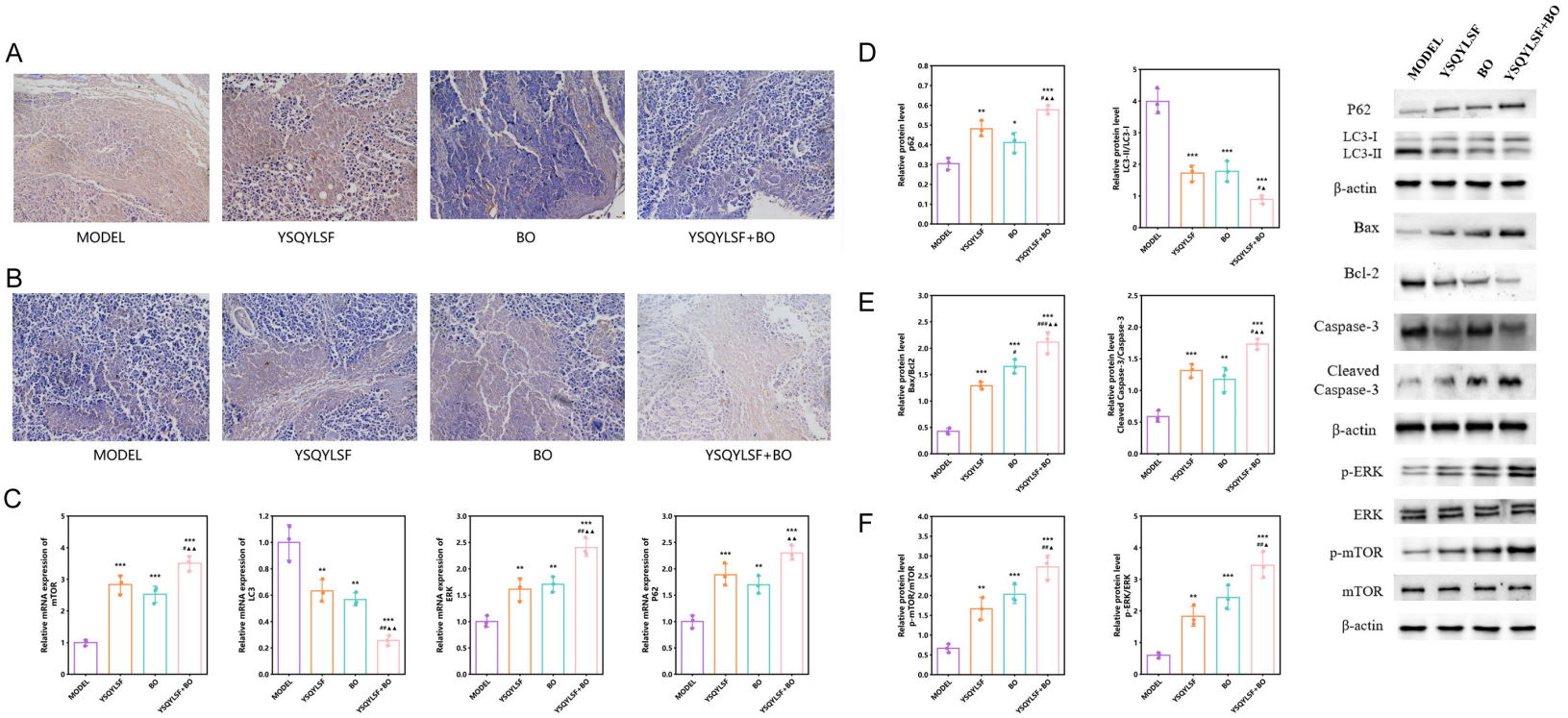

Figure 4. Effects of YSQYLSF and BO on autophagy, apoptosis, and ERK/mTOR signaling in tumor tissues. A. Immunohistochemical staining and quantification of LC3B. B. Immunohistochemical staining and quantification of cleaved caspase-3. C. RT-qPCR analysis of autophagy-related genes. D. Western blot analysis of p62 and LC3B. E. Western blot analysis of Bax, Bcl-2, caspase-3, and cleaved caspase-3. F. Western blot analysis of phosphorylated ERK/ERK and phosphorylated mTOR/mTOR. Data are presented as the mean ± SD (n = 3). *P < 0.05, **P < 0.01, and ***P < 0.001 vs. the Model group; #P < 0.05, ##P < 0.01 vs. the YSQYLSF group; ΔP < 0.05, ΔΔP < 0.01 vs. the BO group.

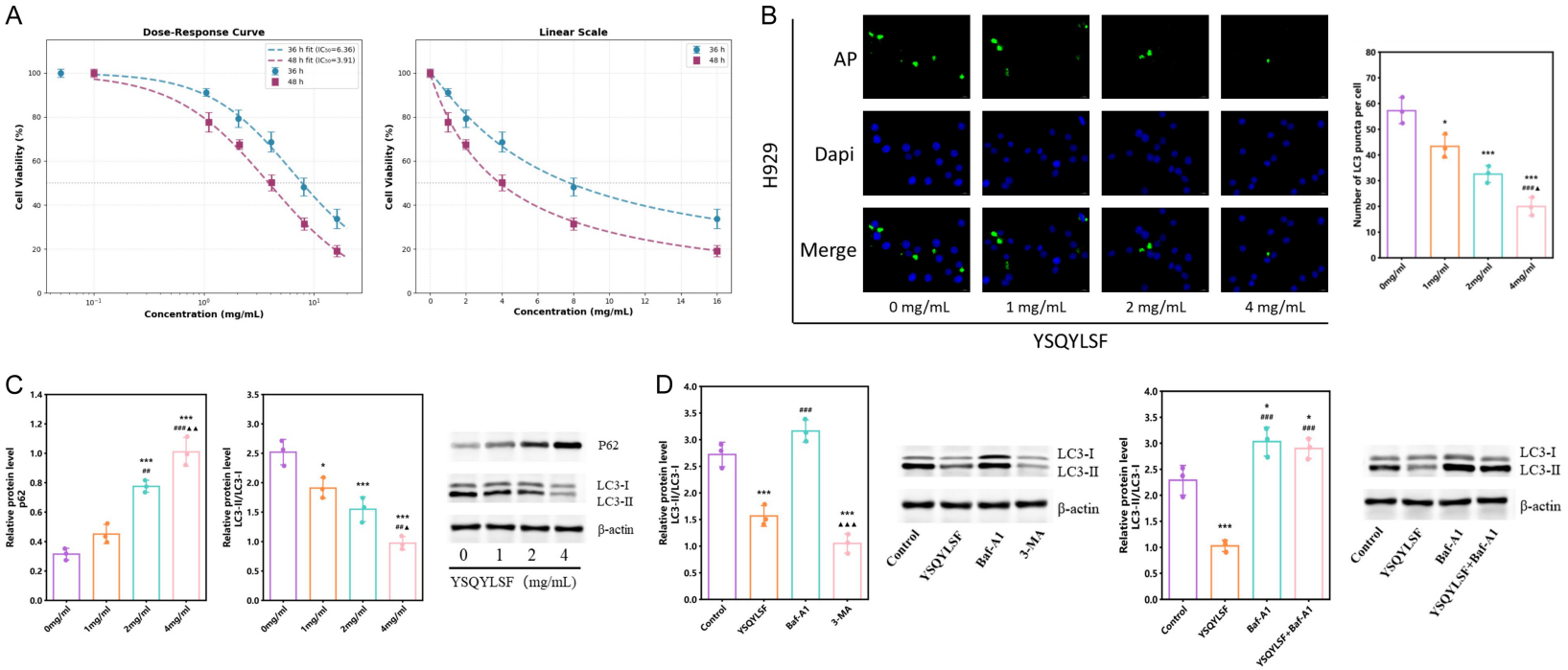

Figure 5. Effects of YSQYLSF on H929 cell proliferation and autophagy. A. Cell viability detected using the 3-(4,5-dimethylthiazol-2-yl)-2,5-diphenyltetrazolium bromide (MTT) assay. B. Green fluorescent protein-LC3 puncta and autophagosome quantification. C. Western blot analysis of p62 and LC3B. D. Effects of YSQYLSF, bafilomycin A1 (Baf-A1), 3-methyladenine (3-MA), and YSQYLSF plus Baf-A1 on the LC3-II/LC3-I ratio. Data are presented as the mean ± SD (n = 3). B, C. *P < 0.05, ***P < 0.001 vs. the 0 mg/mL group; ##P < 0.01, and ###P < 0.001 vs. the 1 mg/mL group; ΔP < 0.05, ΔΔP < 0.01 vs. the 2 mg/mL group. D. *P < 0.05, and ***P < 0.001 vs. the Control group; ###P < 0.001 vs. the YSQYLSF group; ΔΔΔP < 0.001 vs. the Baf-A1 group.

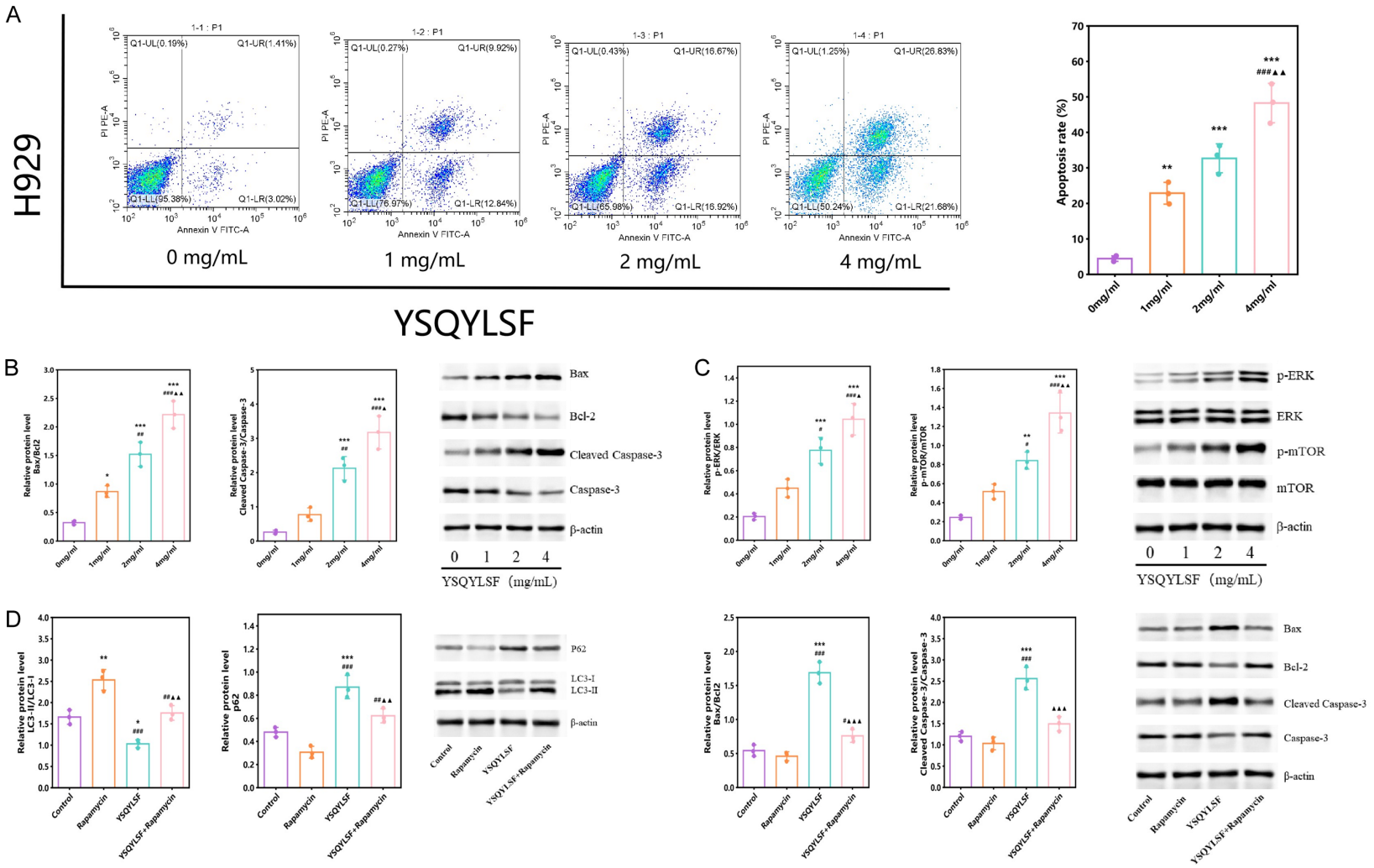

Figure 6. Effects of YSQYLSF on apoptosis and ERK/mTOR signaling in H929 cells. A. Representative flow-cytometry plots and quantitative apoptosis rates based on Annexin V-FITC/PI staining. B. Western blot analysis of apoptosis-related proteins. C. Western blot analysis of phosphorylated ERK/ERK and phosphorylated mTOR/mTOR. D. Effects of rapamycin on autophagy- and apoptosis-related proteins in YSQYLSF-treated H929 cells. Data are presented as the mean ± SD (n = 3). A-C. *P < 0.05, **P < 0.01, and ***P < 0.001 vs. the 0 mg/mL group; #P < 0.05, ##P < 0.01, and ###P < 0.001 vs. the 1 mg/mL group; ΔP < 0.05, ΔΔP < 0.01 vs. the 2 mg/mL group. D. *P < 0.05, **P < 0.01, and ***P < 0.001 vs. the Control group; #P < 0.05, ##P < 0.01, and ###P < 0.001 vs. the Rapamycin group; ΔΔP < 0.01, and ΔΔΔP < 0.001 vs. the YSQYLSF group.

Bcl-2 ratio ($F = 70.41$, $P < 0.001$). Caspase-3 was also significantly cleaved and activated, and the cleaved caspase-3/caspase-3 ratio increased with drug concentration ($F = 53.14$, $P < 0.001$). At 4 mg/mL, the Bax/Bcl-2 ratio reached 2.22 ± 0.24 and the cleaved caspase-3/caspase-3 ratio reached 3.17 ± 0.48, both of which were markedly higher than those in the control group (**Figure 6B**).

Regulation of the ERK/mTOR signaling pathway: Western blot analysis revealed that YSQYLSF increased phosphorylated ERK and mTOR levels in a dose-dependent manner. The p-ERK/ERK ratio ($F = 42.59$, $P < 0.001$) and p-mTOR/mTOR ratio ($F = 45.26$, $P < 0.001$) were significantly elevated in the drug-treated groups. At 4 mg/mL, the p-ERK/ERK ratio increased from 0.20 ± 0.03 to 1.04 ± 0.14, and the p-mTOR/mTOR ratio increased from 0.24 ± 0.02 to 1.34 ± 0.21 (**Figure 6C**).

Rapamycin rescue experiments showed that rapamycin alone significantly downregulated p62 expression and increased the LC3-II/LC3-I ratio. Autophagy levels in the YSQYLSF+rapamycin group were higher than those in the YSQYLSF monotherapy group, as indicated by reduced p62 expression and an increased LC3-II/LC3-I ratio. More importantly, restoration of autophagy significantly inhibited the YSQYLSF-induced increase in apoptosis-related indicators, including the Bax/Bcl-2 and cleaved caspase-3/caspase-3 ratios (**Figure 6D**). These results confirm that YSQYLSF inhibits autophagy and promotes apoptosis through activation of the ERK/mTOR signaling pathway.

Discussion

MM cells are highly dependent on proteostasis, basal autophagy, and stress-adaptive signaling [7]. Although BO has expanded treatment options for MM, relapse, drug resistance, and treatment-related toxicity remain major clinical challenges [8]. In this study, YSQYLSF inhibited H929 xenograft growth, and its combination with BO produced a stronger antitumor effect without obvious body-weight loss or histological evidence of liver or kidney injury [9]. These findings suggest that YSQYLSF may improve therapeutic efficacy when combined with existing antimyeloma agents [10]. The transcriptomic and validation data also raise an important issue regarding ERK/MAPK activation [11]. ERK/MAPK signaling is usually regarded as a growth-promoting pathway in tumor biology [12]; however, its downstream effects are context dependent and are influenced by signal intensity, duration, crosstalk with mTOR, cellular stress status, and the requirement for protective autophagy [13]. In the present study, ERK/mTOR activation was accompanied by decreased LC3-II/LC3-I, p62 accumulation, reduced GFP-LC3 puncta, increased Bax/Bcl-2, enhanced cleaved caspase-3, and partial reversal by rapamycin [14]. Therefore, the observed ERK/mTOR activation is more consistent with a stress-related signal that suppresses protective autophagy and promotes apoptosis than with a simple pro-proliferative event. Further experiments using ERK inhibitors or ERK knockdown are needed to determine whether ERK activation is required for mTOR activation in this model [15]. The mg/mL IC50 values for YSQYLSF should also be interpreted cautiously because the formula is a crude herbal decoction, and the in vitro concentrations represent crude drug equivalents rather than concentrations of a single purified active compound [16]. These IC50 values therefore cannot be directly translated into achievable plasma concentrations after oral administration [17]. In vitro assays were used primarily to determine active concentration ranges and explore mechanisms, whereas oral administration in the mouse xenograft model independently demonstrated antitumor activity [18]. Future pharmacokinetic studies using liquid chromatography-mass spectrometry are necessary to quantify absorbed prototype compounds and metabolites and to establish exposure-response relationships [19]. Transcriptomic analysis identified changes not only in autophagy-, apoptosis-, MAPK-, and mTOR-related pathways but also in immune and inflammatory pathways, including interleukin-17 and Toll-like receptor signaling [20]. Because RNA-Seq was performed on bulk xenograft tumor tissues, these signals may reflect both tumor cell-intrinsic inflammatory programs in H929 cells and contributions from host microenvironmental cells [21].

Although nude mice lack mature T-cell immunity, innate immune cells such as macrophages, neutrophils, natural killer cells, and stromal cells may still infiltrate xenograft tumors and contribute to immune-related signatures; this possibility cannot be excluded under the cur-

rent alignment strategy [22-24]. Future work should combine mouse-human dual-species RNA-Seq analysis, immune deconvolution, immunofluorescence or immunohistochemistry for F4/80, CD11b, Ly6G, NKp46, and CD31, and ideally single-cell RNA-Seq to clarify whether YSQYLSF remodels the tumor immune microenvironment [25]. Other enriched pathways that were not experimentally validated in this study should be interpreted as hypothesis-generating findings, because the present validation focused on ERK/mTOR-mediated autophagy and apoptosis supported by RNA-Seq, GSEA, Western blotting, GFP-LC3 imaging, flow cytometry, IHC, and rapamycin rescue experiments [26, 27]. Nevertheless, inflammatory, immune, and microenvironment-related pathways may represent additional mechanisms of YSQYLSF, and this point has been added to avoid restricting the interpretation of transcriptomic data to a single signaling axis. Several limitations should be acknowledged, including the inability of the subcutaneous xenograft model to fully reproduce the MM bone marrow niche, the use of only one MM cell line for cellular validation, the lack of formal synergy quantification for YSQYLSF plus BO, the unclear material basis and direct molecular targets of YSQYLSF, and the need for additional validation of immune and inflammatory pathway enrichment.

In summary, this study demonstrates that YSQYLSF inhibits MM growth by activating the ERK/mTOR signaling axis, suppressing protective autophagy, and inducing mitochondrial apoptosis. When combined with BO, YSQYLSF further enhanced the antitumor effect while maintaining good tolerability. The enrichment of immune- and inflammation-related pathways suggests that YSQYLSF may have additional effects on the tumor microenvironment that warrant further investigation.

Acknowledgements

This work was supported by the following: 1. Guizhou State Administration of Traditional Chinese Medicione: Effects of Fuzheng Toudu therapy on the Autophagy pathway in MDR/MRD mice (NO.QZYY-2023-016); 2. General Medical Research Fund project: Investigation of the effect of Fuzheng Toudu therapy on MDR by inhibiting the antoph-agy pathway in mice (NO.TYYLKYJJ-2023-035); 3. Hematology Department, Guihang Guiyang Hospital Research Fund project: Investigation of effect of Fuzheng Toudu therapy on MRD-L by inhibiting the antophagy pathway in (No. GHGYYY-KYLX-2023-01).

Disclosure of conflict of interest

None.

Abbreviations

MM, multiple myeloma; YSQYLSF, Yishen Quyu Lishi Formula; BO, bortezomib; ERK, extracellular signal-regulated kinase; mTOR, mammalian target of rapamycin; MAPK, mitogen-activated protein kinase; RNA-Seq, ribonucleic acid sequencing; DEG, differentially expressed gene; GO, Gene Ontology; KEGG, Kyoto Encyclopedia of Genes and Genomes; GSEA, gene set enrichment analysis; RT-qPCR, reverse transcription quantitative polymerase chain reaction; IHC, immunohistochemistry; H&E, hematoxylin and eosin; MTT, 3-(4,5-dimethylthiazol-2-yl)-2,5-diphenyltetrazolium bromide.

Address correspondence to: Xiujun Li, Hematology Department, Guihang Guiyang Hospital, No. 420, Huanghe Road, Xiaohe District, Guiyang 550006, Guizhou, China. Tel: +86-0851-83833093; E-mail: lixiujun740801@163.com

References

[1] Wang S, Xu L, Feng J, Liu Y, Liu L, Wang J, Liu J, Huang X, Gao P, Lu J and Zhan S. Prevalence and incidence of multiple myeloma in urban area in China: a national population-based analysis. Front Oncol 2020; 9: 1513.

[2] Facon T, Dimopoulos MA, Leleu XP, Beksac M, Pour L, Hájek R, Liu Z, Minarik J, Moreau P, Romejko-Jarosinska J, Spicka I, Vorobyev VI, Besemer B, Ishida T, Janowski W, Kalayoglu-Besisik S, Parmar G, Robak P, Zamagni E, Goldschmidt H, Martin TG, Manier S, Mohty M, Oprea C, Brégeault MF, Macé S, Berthou C, Bregman D, Klippel Z and Orlowski RZ; IMROZ Study Group. Isatuximab, bortezomib, lenalidomide, and dexamethasone for multiple myeloma. N Engl J Med 2024; 391: 1597-1609.

[3] Durie BGM, Hoering A, Abidi MH, Rajkumar SV, Epstein J, Kahanic SP, Thakuri M, Reu F, Reynolds CM, Sexton R, Orlowski RZ, Barlogie B and Dispenzieri A. Bortezomib with lenalidomide and dexamethasone versus lenalidomide and dexamethasone alone in patients with newly diagnosed myeloma without intent for immedi-

ate autologous stem-cell transplant (SWOG S0777): a randomised, open-label, phase 3 trial. Lancet 2017; 389: 519-527.
[4] Clavero E, Sanchez-Maldonado JM, Macauda A, Ter Horst R, Sampaio-Marques B, Jurczyszyn A, Clay-Gilmour A, Stein A, Hildebrandt MAT, Weinhold N, Buda G, García-Sanz R, Tomczak W, Vogel U, Jerez A, Zawirska D, Wątek M, Hofmann JN, Landi S, Spinelli JJ, Butrym A, Kumar A, Martínez-López J, Galimberti S, Sarasquete ME, Subocz E, Iskierka-Jażdżewska E, Giles GG, Rybicka-Ramos M, Kruszewski M, Abildgaard N, Verdejo FG, Sánchez Rovira P, da Silva Filho MI, Kadar K, Razny M, Cozen W, Pelosini M, Jurado M, Bhatti P, Dudzinski M, Druzd-Sitek A, Orciuolo E, Li Y, Norman AD, Zaucha JM, Reis RM, Markiewicz M, Rodríguez Sevilla JJ, Andersen V, Jamroziak K, Hemminki K, Berndt SI, Rajkumar V, Mazur G, Kumar SK, Ludovico P, Nagler A, Chanock SJ, Dumontet C, Machiela MJ, Varkonyi J, Camp NJ, Ziv E, Vangsted AJ, Brown EE, Campa D, Vachon CM, Netea MG, Canzian F, Försti A and Sainz J. Polymorphisms within autophagy-related genes as susceptibility biomarkers for multiple myeloma: a meta-analysis of three large cohorts and functional characterization. Int J Mol Sci 2023; 24: 8500.
[5] Dou X, Duan G, Zhong Y, Liu Y, Peng N, Wen L, Qi J, Zhou M, Zhang X and Lu J. The burden of multiple myeloma in China: Trends from 1990 to 2021 and forecasts for 2050. Cancer Lett 2025; 611: 217440.
[6] Boussi LS, Avigan ZM and Rosenblatt J. Immunotherapy for the treatment of multiple myeloma. Front Immunol 2022; 13: 1027385.
[7] George MY, Dabour MS, Rashad E and Zordoky BN. Empagliflozin alleviates carfilzomib-induced cardiotoxicity in mice by modulating oxidative stress, inflammatory response, endoplasmic reticulum stress, and autophagy. Antioxidants (Basel) 2024; 13: 671.
[8] Jiang MZ, Li C, Mao CM, Yu H, Zhou YC, Pu SQ, Li RZ, Liao YJ, Zhang DY, Yang P, Li MH and Li M. The MAPK/ERK signaling pathway involved in Raddeanin A induces apoptosis via the mitochondrial pathway and G2 phase arrest in multiple myeloma. Sci Rep 2024; 14: 29061.
[9] Liu NA, Liu JQ, Liu Y, Zhu Q, Zheng D, Li F, Meng LZ and Qiu M. Rehmannia glutinosa polysaccharide regulates bone marrow microenvironment via HIF-1α/NF-κB signaling pathway in aplastic anemia mice. An Acad Bras Cienc 2023; 95: e20220672.
[10] Kim J, Kundu M, Viollet B and Guan KL. AMPK and mTOR regulate autophagy through direct phosphorylation of Ulk1. Nat Cell Biol 2011; 13: 132-141.
[11] White E and DiPaola RS. The double-edged sword of autophagy modulation in cancer. Clin Cancer Res 2009; 15: 5308-5316.
[12] Janku F, McConkey DJ, Hong DS and Kurzrock R. Autophagy as a target for anticancer therapy. Nat Rev Clin Oncol 2011; 8: 528-539.
[13] Dai H, Ma B, Dai X, Pang J, Wang J, Zhao Y, Wang M, Zhang H, Gao H, Qian S, Tian F and Sun X. Shengma biejia decoction inhibits cell growth in multiple myeloma by inducing autophagy-mediated apoptosis through the ERK/mTOR pathway. Front Pharmacol 2021; 12: 585286.
[14] Yimingniyazi N, Abudureheman M, Aili W, Abudurexiti N, Rouzi N, Abudureyimu A and Abudureheman A. BRMS1 suppresses the PI3K/AKT/mTOR pathway to regulate autophagy in multiple myeloma. Leuk Lymphoma 2025; 66: 2097-2107.
[15] Zhang R, Yang X, Shi X, Xing E, Wang L, Hao C and Zhang Z. Bortezomib modulated the autophagy-lysosomal pathway in a TFEB-dependent manner in multiple myeloma. Leuk Res 2024; 138: 107455.
[16] Sarafraznia L, Tahan Nejad Asadi Z, Dayer D, Jalalifar MA and Ghanatir N. Investigation of non-coding RNA-related autophagy alterations in drug-resistant multiple myeloma plasma cells. Iran J Pathol 2024; 19: 422-430.
[17] Fulton-Ward T, Gudgeon N, Thirlwell I, Bishop EL, Marzullo B, Giles H, McIlroy G, Ferguson P, Kishore B, Rogers K, Alfasi N, Wong T, Aytain S, Tennant DA, Pratt G and Dimeloe S. mTOR activity and metabolic reprogramming of CD8+ T cells is impaired under hypoxia and within the multiple myeloma bone marrow. Blood Adv 2025; 9: 6175-6188.
[18] Autophagy Guidelines Group. Guidelines for the use and interpretation of assays for monitoring autophagy (4th edition)[1]. Autophagy 2021; 17: 1-382.
[19] Kapoor S, Gupta N and Sharma A. A polyherbal ashwagandha formulation exhibits adjunctive antitumor efficacy against u266 myeloma cells by multi-strategic cytotoxic effects: an experimental approach. Asian Pac J Cancer Prev 2023; 24: 3705-3714.
[20] Zhang RJ, Wang ZL, Shi XM, Zhang SY, Wang W, Ma MS, Li C, Gu CH and Zhang ZH. The role and molecular mechanism of transcription factor EB and its target genes in multiple myeloma treatment with bortezomib. Zhonghua Xue Ye Xue Za Zhi 2025; 46: 1052-1059.
[21] Kudalkar R, Altom J, Galloway J, Manning V, Taranto S and Cottini F. Regulation of stress tolerance by CREB1 sustains multiple myeloma cell survival. Cell Death Dis 2026; 17: 46.
[22] Wu X, Liu Y, Zhang E, Chen J, Huang X, Yan H, Cao W, Qu J, Gu H, Xu R, He J and Cai Z. Dihy-

droartemisinin modulates apoptosis and autophagy in multiple myeloma through the P38/MAPK and Wnt/β-catenin signaling pathways. Oxid Med Cell Longev 2020; 2020: 6096391.

[23] Lezama RA, Gudiño García A, López Ramírez K, Vela Ojeda J, Reyes Maldonado E and Victoria-Avila ZL. Mechanism regulation of endoplasmic reticulum stress in multiple myeloma cells: modulation of the UPR, UPS, autophagy, HSPs, and potential therapeutic targets. Expert Rev Hematol 2026; 19: 143-156.

[24] Hideshima T, Richardson PG and Anderson KC. Mechanism of action of proteasome inhibitors and deacetylase inhibitors and the biological basis of synergy in multiple myeloma. Mol Cancer Ther 2011; 10: 2034-2042.

[25] Dhakal B, Hari P, Chhabra S, Szabo A, Lum LG, Glass DD, Park JH, Donato M, Siegel DS, Felizardo TC and Fowler DH. Rapamycin-resistant polyclonal Th1/Tc1 cell therapy (RAPA-201) safely induces disease remissions in relapsed, refractory multiple myeloma. J Immunother Cancer 2025; 13: e010649.

[26] Yang ZJ, Chee CE, Huang S and Sinicrope FA. The role of autophagy in cancer: therapeutic implications. Mol Cancer Ther 2011; 10: 1533-1541.

[27] Li J, Gao Y, Ren X, Li Y, Wu L, Yang X, Wang J, Shang H, Xiong X and Xing Y. The role of biologically active ingredients from Chinese herbal medicines in the regulation of autophagy in treating cardiovascular diseases and other chronic diseases. Curr Pharm Des 2017; 23: 1060-1069.